Overview of the KSTAR research progress and future plan toward ITER and K-DEMO*

H.K. PARK[a], M.J. CHOI[b], S.H. HONG[b] Y. In[a], Y.M. JEON[b], J.S. KO[b], W.H. KO[b], J.G. KWAK[b] J.M. KWON[b], J. Lee[b], J.H. LEE[b], W. LEE[b], Y.B. NAM[d], Y.K. OH[e], B.H. PARK[b], J.K. PARK[f], Y.S. PARK[g], S.J. WANG[b], M. YOO[c], S.W. YOON[b], J.W. AHN[h], J.G. BAK[b], C.S. CHANG[f], W.H. CHOE[i], Y. CHU[b], J. CHUNG[b], N. EIDIETIS[j], H.S. HAN[b], S.H. HAHN[b], H.G. JHANG[b], J.W. JUHN[b], J.H. KIM[b], K. KIM[h], A. LOARTE[e], H.H. LEE[b], K.C. LEE[b], D. MUELLER[f], Y.S. NA[c], Y.U. NAM[b], G.Y. PARK[b], K.R. PARK[b], R.A. PITTS[e], S.A. SABBAGH[g], G.S. YUN[k], AND THE KSTAR TEAM

[a] Ulsan National Institute of Science and Technology, Ulsan, Korea
[b] National Fusion Research Institute, Daejeon, Korea
[c] Seoul National University, Seoul, Korea
[d] CEA, St. Paul Lez Durance, France
[e] ITER Organization, Route de Vinon-sur Verdon. 13067 St. Paul Lez Durance, France
[f] Princeton Plasma Physics Laboratory, Princeton, NJ, USA
[g] Columbia University, NY, USA
[h] Oak Ridge National Laboratory, TN, USA
[i] Korea Advanced Institute of Science and Technology, Daejeon, Korea
[j] General Atomics, CA, USA
[k] Pohang University of Science and Technology, Pohang, Korea
e-mail: hyeonpark@unist.ac.kr

Abstract

A decade long operation of KSTAR has contributed significantly to operation of superconducting tokamak device and advancement of tokamak physics which will be beneficial for the ITER and K-DEMO programs. Even with limited heating capability, various conventional as well as new operating regimes with new start-up methods have been explored and achieved great performance. As examples, a long pulse H-mode operation with and without the ELM-crash was well over 60 seconds and over 30 seconds, respectively. Unique capabilities of KSTAR allowed to improve control capability of harmful instabilities and have been instrumental for many exciting new physics. The intricate IVCC system was a great perturbation tool in studying of threshold power of the L/H transition in the presence of non-axisymmetric fields, rotation physics due to NTV effects and heat dispersal in divertor system and predictive control of the ELM-crash with a priori modeling. The state-of-the-art 2D/3D microwave imaging systems uncovered many new exciting physics in the MHD and turbulence transport area. They are validation of $q_0>1$ right after the sawtooth crash, self-consistent asymmetric distribution of plasma turbulence amplitude and flow in the presence of 2/1 island, and underlying physics of low frequency turbulence induced by 3D resonant fields in suppression of the ELM-crash through non-linear interaction with the ELMs. In the turbulence area, non-diffusive "avalanche" transport event and role of quiescent coherent mode in ohmic confinement are studied. To accommodate anticipating higher performance of the KSTAR plasmas with increased heating powers (NBI and ECH), new divertor/internal interface with full active cooling system will be implemented after the increased heating power system and a new current drive system are fully tested. Upgrade plan for the internal hardware and efficient current drive system may allow a long pulse operation of higher performance plasmas at $\beta_N>3.0$ with $f_{bs}\sim0.5$ and $T_i>10$keV.

1. INTRODUCTION

The mission of the Korean Superconducting Tokamak Advanced Research (KSTAR) is to achieve construction and operation experience of superconducting tokamak device and explore the physics and technology of high performance steady state operation that are essential for ITER and fusion reactors.[1] Through experimental campaigns on KSTAR for a decade, the machine limit has been explored with limited ancillary systems and relevant technology of the superconducting tokamak has been improved for the KSTAR operating space, as well as support for ITER and K-DEMO [2] programs. The achieved performances in recent campaigns, operation boundary and future direction are illustrated in Fig. 1 and machine parameters of KSTAR (design and achieved values) are compared with those of ITER and K-DEMO in Table.1. Various operating regimes with the corresponding achieved performances are; high β_p (up to ~2.8) non-inductive long pulse up to ~8s, high β_N up to ~ 4.3 (transient value), low edge q_{95} at ~2.3, elongation of ~2.16 which exceeded the design value and stable Internal Transport Barrier (ITB) mode up to ~7s. Note that the confinement of the ITB mode is compatible to that of the H-mode. New start-up scenario utilizing turbulent ExB mixing avalanche was developed. The pulse length of the H-mode discharge with and without edge localized mode (ELM)-crash has been extended to over a minute and half minute, respectively.

Along with the performance enhancement in various operating regimes, validation of critical physics and study of improved stability and confinement of the plasma have been pursued utilizing three unique features of KSTAR.

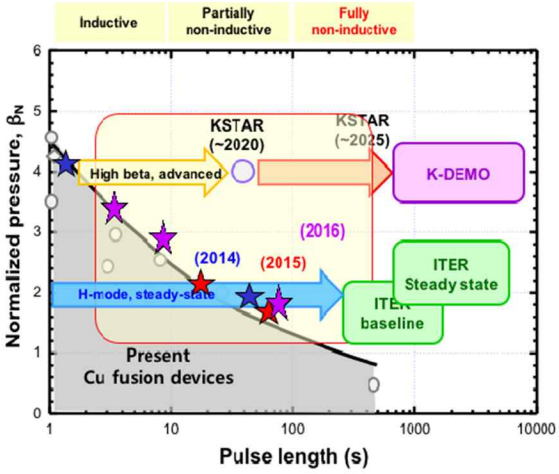

Fig. 1. The achieved operation boundary of KSTAR is illustrated in a space spanned by β_N and pulse length. With the upgraded ancillary systems, a longer pulse with higher β_N will be attempted to support ITER and K-DEMO programs

Parameters	KSTAR (achieved)	ITER (Baseline)	K-DEMO (Option II)
Major radius, R_0 [m]	1.8 (←)	6.2	6.8
Minor radius, a [m]	0.5 (←)	2.0	2.1
Elongation, κ	2.0 (2.16)	1.7	1.8
Triangularity, δ	0.8 (←)	0.33	0.63
Plasma shape	DN, SN	SN	DN (SN)
Plasma current, I_P [MA]	**2.0 (1.0)**	15	> 12
Toroidal field, B_0 [T]	**3.5** (←)	5.3	7.4
H-mode duration [sec]	**300 (70)**	**400**	**SS**
β_N	**5.0 (4.3)**	**~ 2.0**	**~ 4.2**
Bootstrap current, f_{bs}	**(~0.5)**		**~ 0.6**
Superconductor	Nb_3Sn, NbTi	Nb_3Sn, NbTi	Nb_3Sn, NbTi
Heating /CD [MW]	**~ 28 (10)**	~ 73	120
PFC	C, W	W	W
Fusion power, P_{th} [GW]		~0.5	~ 3.0

Table. 1. KSTAR machine parameters are compared with those of ITER and K-DEMO

They are a plasma with nearly perfect toroidal symmetry [3], robust magnetic perturbation tool [4] and state-of-the-art 2D/3D microwave imaging diagnostics [5, 6]. The nearly perfect axisymmetry of the KSTAR plasma (magnetic ripple of 0.04% and error field, $\delta B/B_0 \sim 1x10^{-5}$) results in extremely high toroidal rotation speed with strong edge shear which may influence the confinement and stability of the plasma. The robust in-vessel control coil (IVCC) system with n=1 and 2 resonant toroidal mode numbers has been instrumental for studying underlying physics of the resonant and non-resonant magnetic perturbation (RMP and NRMP) for control of the harmful instabilities and physics experiments. Successful suppression experiment of the ELM-crash with a priori modeling with the optimum phase and amplitude of the RMP coil current was successfully carried out [7]. Here, the results suggested that inclusion of the plasma response in modeling is critical. Also empirical study of the L/H transition threshold power (P_{th}) dependence on non-axisymmetric 3D field demonstrated that the P_{th} is sensitive to RMP but insensitive to NRMP [8].

In study of new physics, the long-standing conundrum of q_0 in sawtooth instability in the core of the plasma was revisited. Here, a definitive validation of $q_0>1.0$ after the sawtooth crash (i.e., "full reconnection model") was achieved based on direct measurement assisted by supplementary experiment [9]. Also, it is demonstrated that the crash time scale of the sawtooth instability can be slowed by an order of magnitude [10]. The measured asymmetric 2D electron temperature (T_e) turbulence and poloidal shear flow pattern in the presence of macroscopic island (m/n=2/1) [11] were consistent with the results from the modeling based on XGC and gyrokinetic codes) [12]. Suppression of the ELM-crash with RMP was interpreted due to non-linear interaction between the ELMs and low frequency turbulence induced by the penetrated 3D field of RMP [13]. In addition, the observed timing of the ELM-crash suppression is well correlated the critical amplitude of turbulence as well as a sudden reduction of the perpendicular rotation velocity of the turbulence. The perpendicular rotation reduction is found to be mainly due to sudden change of E_r [14]. An "avalanche", non-diffusive local transport event, was observed in both L-mode and ITB plasmas and detail analysis is in progress [15]. In electron density fluctuation measurement, quasi-coherent modes (QCMs) were measured with the MIR system and may play an important role in ohmic confinement physics [16]. In the 2018 campaign, a 2nd NBI system will be commissioned and the first 2MW power will expand the operation regimes and performance of the plasmas. The additional heating capability [2nd NBI power (6MW) with ECH power (~4MW)] will be fully tested prior to upgrade plan for new divertor and internal structure with active cooling. The upgrade plan is scheduled in ~2021. Then, plasma operation regimes with enhanced beta can be fully tested with new divertor system. With the best suited current drive system, higher beta long pulse operation that is essential for the goal of KSTAR as well as ITER and K-DEMO will be realized.

2. KSTAR AS A UNIQUE RESEARCH TOKAMAK DEVICE

When the concept of KSTAR was conceived as a superconducting tokamak device capable of steady state operation, the imposed engineering constraints were extremely stringent. To achieve a near perfect toroidal

symmetry of the plasma, the first consideration was to minimize the toroidal magnetic ripple, which is known to be harmful for trapped particles, to ~0.04% level at the outer edge of the plasma. The second effort was a precise design and alignment of the superconducting coils to minimize the error fields, which were known as a potential source of instabilities and poor particle confinement [17, 18]. As the KSTAR started the operation in 2008, the magnetic field ripple and n=1 non-axisymmetric magnetic field component were measured to be ~5 x 10^{-4} and ~1 x 10^{-5}, respectively. The measured $\delta B/B_0$ data up to ~4 x 10^{-5} at the plasma β_N=2 together with the level of error fields in other devices including the projected ITER value are shown in Fig. 2 [3]. Note that this value is ~20% below the design value of ITER. The nearly perfect toroidal symmetry of the plasma in KSTAR provides an excellent opportunity to revisit the confinement and stability physics that might be affected by the non-axisymmetric fields of the plasma.

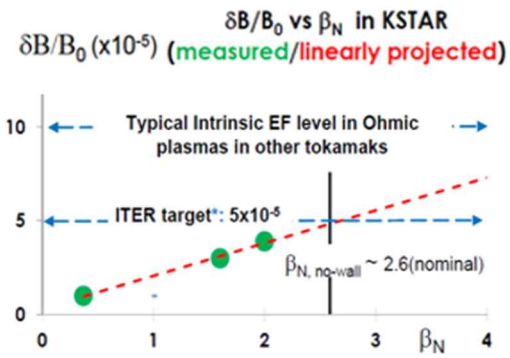

Fig. 2. The projected error field fraction of KSTAR is shown as a function of plasma β_N. Even at β_N~2, the error field is lower than the ITER target value.

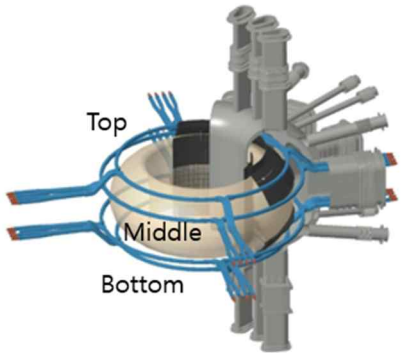

Fig. 3. Three rows of IVCC assembly (top, middle and bottom) with picture frame type two turns is equipped with fast control power supply system.

For perturbative physics experiments and control of MHD instabilities on KSTAR, a robust magnetic perturbation tool with the resonant toroidal mode number of n=1 and 2 was designed and installed as depicted in Fig. 3. The In-Vessel Control Coils (IVCC) consist of three rows (top, middle, and bottom) with 2 turns in the low field side of the device is shown in this figure. The philosophy of the low n system on KSTAR was based on possible external coil system for the future reactor. A broadband power supply system capable of switching up to ~1 kHz in DC is equipped and has been used for fast control of MHDs with various 3-D configuration of the coils. Note that the ITER IVCC design has also three rows like KSTAR with n=3 and 4 resonant mode and experiences in perturbative physics experiment in KSTAR will be beneficial for performance of the ITER IVCC system.

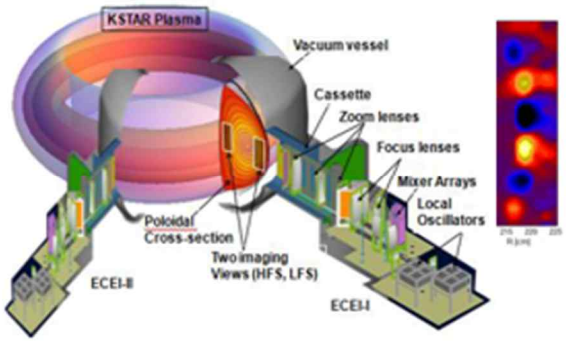

Fig. 4. The ECEI-I is toroidally separated by 22.9^0 from ECEI-II and the MIR system is combined with the ECEI-II system. A typical images of the ELM structures at low field side is shown.

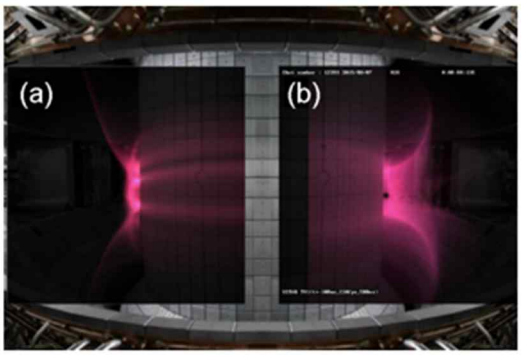

Fig. 5. Comparison of a synthetic diagnostic of the Balmer-α line emission in the BREAK code simulation considering the self-generated electric fields (a) with an experimental visible camera image (b) from KSTAR

The last unique feature of KSTAR is the most advanced 2D/3D microwave imaging diagnostics as shown in Fig. 4. They are Electron Cyclotron Emission Imaging (ECEI) system [5] for electron temperature (T_e) fluctuation and Microwave Imaging Reflectometry (MIR) system [6] for electron density (n_e) fluctuation measurement. Two ECEI systems (ECEI-I and ECEI-II) are capable of measuring three simultaneous images of T_e fluctuations (two

simultaneous images on the same poloidal plane and one image toroidally separated by 22.9^0 as shown in Fig. 4. Each image consists of 192 pixels with vertical zoom capability up to a factor of three and nominal pixel size is ~1.2cm (radial) by ~1.2cm (vertical) and vertical pixel can size can be enlarged up to ~3 cm and the radial size will be slightly increased (~2 cm) and decreased (~1 cm) due to fixed frequency band of the detection system in a varying magnetic field (B~1/R). MIR system (total 64 channels) is capable of simultaneously measuring n_e fluctuations at four reflection layers with 16 poloidal positions at each layer.

3. EXPLORATION OF OPERATING REGIMES AND PARAMETER EXPANSION

During the last two KSTAR campaigns (2016 and 2017), research effort accelerated exploration of plasma operating regimes that could be potentially beneficial for ITER and K-DEMO [2]. A novel plasma breakdown theory of turbulent ExB mixing avalanche has been developed and validated against KSTAR experiments as shown in Fig. 5. It was found that the self-generated electric fields play important role to reduce the avalanche growth rate and cause a dominant perpendicular transport via ExB drift during the breakdown [19]. A more robust and efficient plasma start-up scheme has been established in KSTAR by replacing the conventional Field Null Configuration (FNC) by Trapped Particle Configuration (TPC), which has significantly improved the initial formation of the density and plasma current [20] and widened the operation window of start-up plasmas and can easily be applied to ITER. Enhanced performance in various operating regimes was obtained and machine parameters were expanded. Examples, like high β_p (up to ~2.8) non-inductive long pulse up to ~8s, high β_N regime up to ~ 4.3, long pulse high beta hybrid regime, ITER baseline regime (IBS), internal transport barrier (ITB) mode [21] and regime with extremely low edge q_{95} up to ~2.3 are illustrated with no wall and ideal wall limits of KSTAR in Fig. 6. The pulse length of the H-mode discharge was extended to over a minute at a moderate plasma beta. The improved experimental design using IVCC to suppress the ELM-crash and enhanced understanding of the underlying physics of resonant and non-resonant magnetic perturbation (RMP and NRMP) successfully produced a long pulse (~34s) H-mode without ELM-crash with the n=1 RMPs at P_{NBI}~2.8 MW, I_p=0.56 MA, and B_T=1.8 T

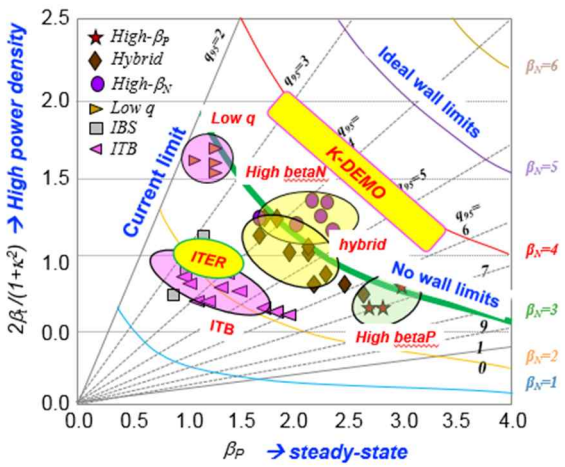

Fig. 6. Various operating regimes were explored for physics understanding and search for ideal operation mode of K-DEMO

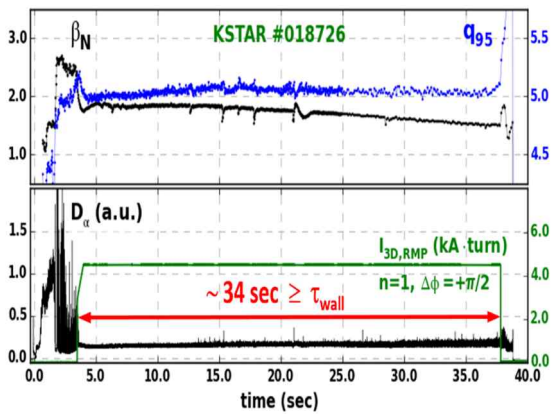

Fig. 7. The longest ELM-crash free H-mode discharge obtained with n=1 RMPs.

as illustrated in Fig. 7. In addition to efforts on improving the performance of conventional modes of operation and long pulse capability, search for alternative operating regime at a low edge q_{95}~2.2 with improved core confinement such as ITB mode with the ITB foot position pushed further out while keeping the edge recycling at low level. Under this mode of operation, the growth rates of NTMs and ELMs can be minimized and only has to deal with the sawtooth instability and perhaps 3/2 mode. In fact, the sawtooth instability can be used for particle exhaust and the size and crash time can be easily controlled with external current profile control. The only drawback may be a reduced bootstrap current at the edge but the price for additional current drive system might be much less than that for the controlling of instabilities such as the ELMs and NTMs, if these instabilities can ever be completely suppressed. For potential basis of the future K-DEMO, an alternative mode with high energy confinement comparable to that of the H-mode with lesser intrinsic harmful instabilities will be pursued and any acceptable alternative operational mode will be explored in KSTAR.

4. NEW RESEARCH RESULTS FROM NEARLY PERFECT AXISYMMETRIC TOKAMAK PLASMAS

In tokamak plasmas, it is well known that the non-axisymmetric magnetic fields (magnetic field ripple and error field) influence the confinement and stability of the plasma. The nearly perfect axisymmetric plasmas in KSTAR are an ideal testbed to review the confinement and stability physics. Among many notable experimental observations, the absence of resistive wall modes (RWMs) even at β_N~4.3 which is above no-wall limit for KSTAR, and exceptionally high toroidal rotation speed for similar level of torques in other devices were notable. Systematic study of physical quantities that might be affected by the intrinsic non-axisymmetric field such as the L/H transition threshold power, energy confinement time and MHD stability limits, etc., was initiated. In the study of the L/H transition threshold power (P_{th}) dependence on the non-axisymmetric field, it was found that the P_{th} is significantly affected by RMPs as shown in Fig. 8(a) while NRMP components had no influence on P_{th} [8] as demonstrated in Fig. 8(b). Here, the P_{th} dependence on $\delta B/B_0$ for resonant component of the n=1(blue) and n=2 (purple) mode is compared with the same dependences at high $\delta B/B_0$ ~10^{-4} (pink). Here, the n=1 $\delta B/B_0$ was fixed at ~2.7x10^{-4} and n=2 component was increased (pink) like some devices with intrinsic error fields at this level. This comparative study suggests that the ITER H-mode operation may not have to be concerned with the non-resonant error field components. Research on disruption prediction, critical for ITER, has begun to be addressed on KSTAR. Another apparent advantage of the nearly perfect axisymmetry of KSTAR is the reduced plasma disruptivity in the Ip flat-top period of the plasma [22].

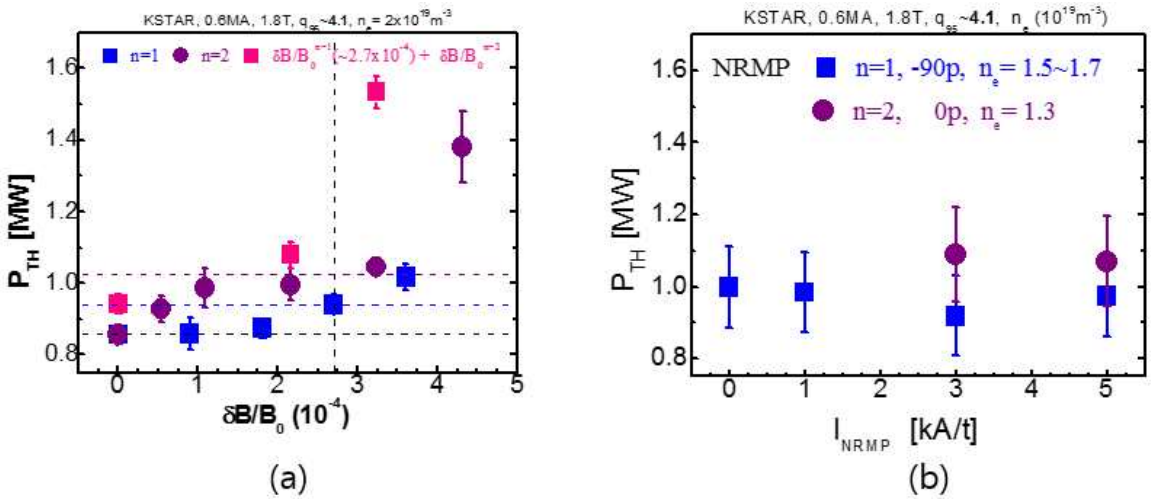

Fig. 8. (a) P_{th} dependence on $\delta B/B_0$ (n=1 and n=2 resonant components) is compared with P_{th} dependence on $\delta B/B_0$ (n=1) of O (~10^{-4}) [n=2 $\delta B/B_0$ component was varied a fixed n=1 $\delta B/B_0$ =~2.7x 10^{-4}]. (b) No dependence of P_{th} on non-resonant component of $\delta B/B_0$ (n=1 and n=2) is demonstrated

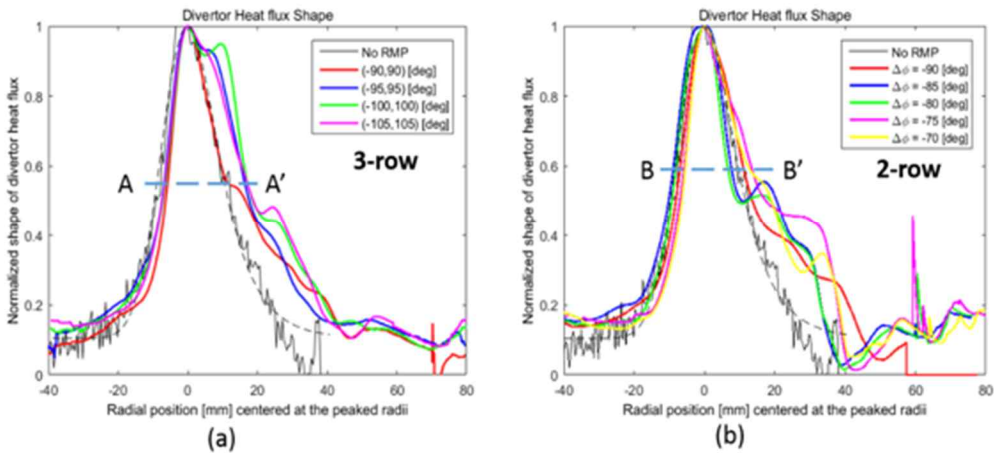

Fig. 9. Shapes of toroidally-averaged divertor heat fluxes in misaligned rotating by RMP configurations with (a) 3-rows (top, middle, bottom) and (b) 2-rows (top and bottom) are shown. Each shape in misaligned rotating RMP configuration is compared with no RMP (black) and typical rotating RMP with n= +90^0 phasing (red)..

Heat dispersal at the divertor is critical issue in high performance discharges. Application of rotating RMPs in KSTAR [23] found that the ITER like 3-row RMPs (top, middle and bottom) have broadened the divertor heat flux in the vicinity of outer strike point as shown in Fig. 9(a), while 2-row RMPs (top and bottom) have rarely affected the near scrape-off layer (SOL) heat flux despite a mildly broadened profile change in the far-SOL area as shown in Fig. 9(b). Note that the widths of A-A' in Fig. 9(a) at the near SOL with 3-rows are broader, while those of B-B' in Fig. 9(b) with 2-rows are rarely broadened. In Fig. 9(a), (ϕ_{Top}, ϕ_{Bot}) refers to the phases of the top and bottom row, while fixing ϕ_{Mid} at 0^0. In Fig. 9(b), each angle is the RMP phase difference between top and bottom rows of IVCCs. Since the divertor heat flux dispersal represents redistribution of the peaked near-SOL heat flux, the ITER RMP is expected to be capable of diffusing the divertor heat flux using intentionally misaligned configurations with minimizing electromagnetic loads on RMP coil, while sustaining the ELM-crash suppression.

A beneficial neoclassical toroidal viscosity (NTV) effect created by an applied 3D field that can be used to generate significant plasma rotation and shear in slowly rotating plasmas such as envisioned in ITER is NTV offset rotation [24]. Past experimental research has only considered that the NTV offset rotation can occur in the direction opposite to the plasma current (counter-I_p). KSTAR experiments have directly measured for the first time the profile of controlled rotation in the co-I_p direction, V_0^{NTV}, by this effect [26]. This is expected by generalized NTV theory allowing for torques generated by both electron and ion channels, the balance of which yields the V_0^{NTV} profile (electron/ion NTV torque scales as $(m_i/m_e)^{0.5}(T_e/T_i)^{3.5}$ indicating that the electron channel can be dominant). The V_0^{NTV} profile was directly measured with no modeling assumptions by applying different 3D field magnitudes (predominantly n = 2) to a sufficiently high level at which saturation to the V_0^{NTV} profile occurs expected by theory. Figure 10 illustrates a progression of V_ϕ profiles in ohmic plasmas and an ECH plasma producing V_0^{NTV} profiles. The intrinsic rotation profile (no applied 3D field) shown under ohmic heating has V_ϕ near zero in the core region, increasing at large R. When the n = 2 applied field is added, rotation in the outer region approximately doubles to 15 km/s. This shows that the rise is due the 3D field and not simply ECH. Additionally, when ECH is added, the heating in the outer region leads to a strong increase of V_ϕ, again more than doubling it to 35 km/s. The rotation in the plasma outer region equates to more than 12 krad/s and is quite significant compared to projections for ITER of approximately 2 krad/s in the pedestal region [26].

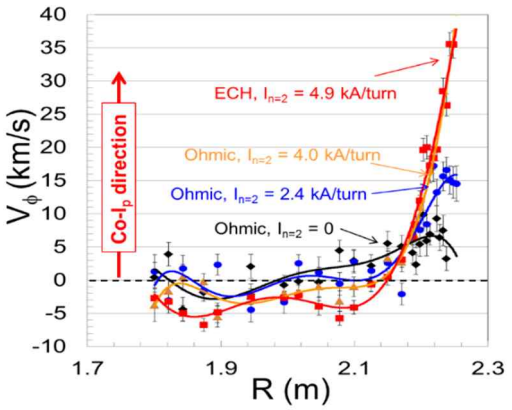

Fig. 10. Comparison of plasma rotation profiles in ohmic and ECH heated plasmas at varied 3D fields. illustrating the strong shear and rotation generated in the co-Ip direction by the generalized NTV offset rotation effect.

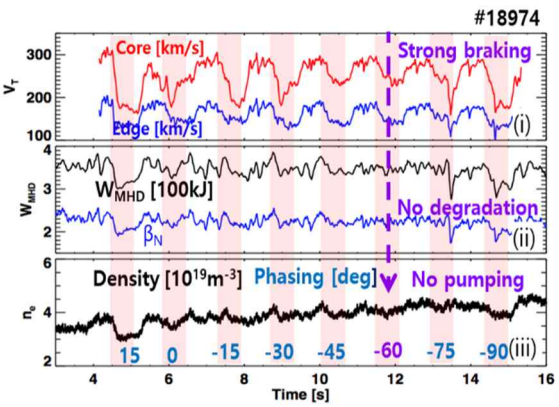

Fig. 11. Demonstration of quiescent configuration: No changes of stored energy and plasma density while rotations at the core and edge are controlled with 3 rows of RMP coils with different phasing

The exclusive separation of dominantly resonant and non-resonant components has been elusive, in that almost all the non-axisymmetric fields, in practice, consists of both components. However, a rigorous benchmarking of NTV theory would be feasible, only when the magnetically distorted flux surface exists without affecting either particle or energy transport. Such conditions have been found using the 3-row IVCC in KSTAR, pinpointing the existence of the 'quiescent' configuration, as shown in Fig. 11 (i.e. near -60^0 phasing). Shown in this figure are the time evolutions of (i) toroidal rotations in core (red) and at edge (blue), (ii) stored energy (black) and normalized-β β_N (blue), and (iii) two-color-interferometry (TCI) line-integrated average of plasma density (n_e), respectively. Note that the experimentally identified 'quiescent' phasing near -60^0 rarely changes either the stored energy or plasma density, in which the plasma rotation is exclusively controlled by strong NTV torque.

5. NEW PHYSICS OF MHD AND TRANSPORT BASED ON TURBULENCE

The KSTAR is an ideal research device for validation of unresolved physics issues as well as exploration of new and/or missing physics of MHD and turbulence with the unique research tools described in previous section. The innovative IVCC system has been used as a perturbation tool for physics studies and the response was monitored by the state-of-the-art 2D/3D microwave imaging diagnostics. The 2D/3D experimental measurements with adequate temporal and spatial resolutions provided comprehensive details of transient and steady state behaviors of MHDs and turbulence and can impose stringent boundary conditions for physics modeling. Reciprocally, any predictive capability of the modeling can be challenged with these unprecedented experimental data. The selected new findings such as the 1/1 kink instability in the core, turbulence behavior in the presence of the 2/1 tearing mode, the ELMs and dynamics during control experiments with RMPs at the pedestal region and turbulence related transport will be addressed in this section.

5.1. VALIDATION OF "FULL RECONNECTION MODEL" OF THE SAWTOOTH INSTABILITY

The m/n=1/1 internal kink (or tearing mode) known as sawtooth in the core of tokamak plasmas and experimental validation of the stability criterion of the internal kink has been controversial for a long time since the measurements of $<q_0>$~0.75 with variation of ~0.05 [27] and $<q_0>$~1.0 with variation of ~0.05 [28] could not validate the proposed full reconnection model [29]. The unresolved central q_0 problem (i.e. full vs. partial reconnection models) was revisited with the sophisticated Motional Stark Effect (MSE) system on KSTAR [30]. In the last two KSTAR campaigns (2015 and 2016), the measured median $<q_0>$ was ~1.0 with variation of ~0.05 in sawtoothing discharges as shown in Fig. 12(a). The difference in $<q_0>$ cannot be reconciled with a possible off-set due to any unknown factors such as intrinsic E_r and shape factor, κ. The small variation of q_0 (~0.05) is universal in all measurements and this is consistent with the expected small diffusion of the equilibrium during the crash. It is necessary to introduce a comprehensive experiment to address the q_0 is above or below ~1.0 right after the crash.

Following the classical off-axis sawtooth event from double tearing mode experiment near q~2 region [31], a supplementary experiment utilizing double tearing modes inside the q=1 surface using current blip with ECCD was conducted. As shown in Fig. 12(b), the current blip is scanned from the center of the plasma to the edge of the q=1 surface. As the current blip is moved from center to edge, double tearing modes with different resonant mode numbers (m/n= 2/2, 3/3, 4/4, 5/5, etc.) were observed right after the crash. During one period of sawtooth oscillation, the excited resonant tearing modes (3/3 or 2/2) transform into the 1/1 tearing mode which leads to the crash as the current profile is further evolved due to T_e rise and accumulation of the injected current. Here, both the location and time evolution of the excited tearing modes were consistent with the growth rates of these modes calculated with the MHD code, M3DC1, in which an equilibrium q profile with q_0=1.04 and modelled current blip were used. Combining with the measured q profile in Fig. 10(a), validation of the full reconnection model (q_0>1.0 after the crash) is conclusive and the off-set can be adjusted to make sense of the measurement.

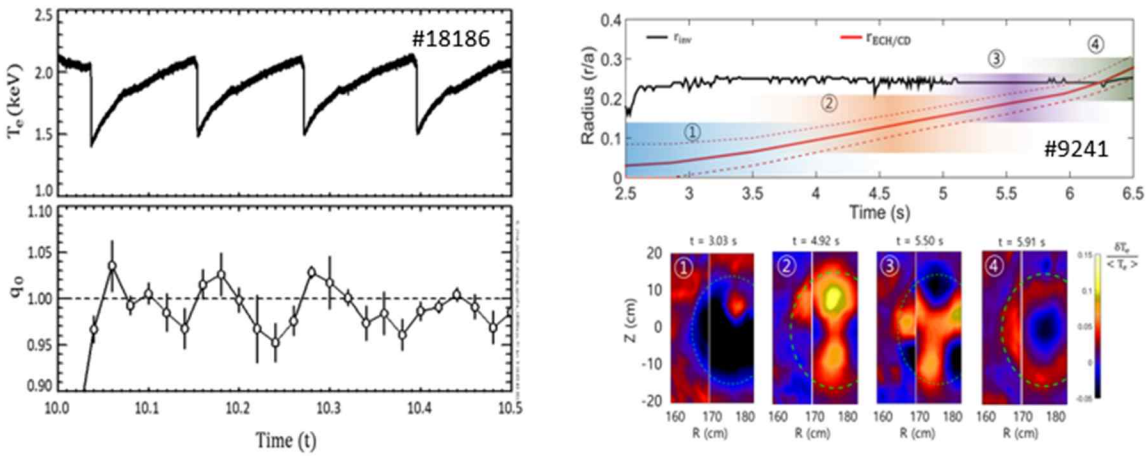

(a) (b)

Fig. 12. (a) The measured time evolution of q_0 by MSE system during sawtooth oscillation shows that $<q_0>$ is ~1.0 with small variation of ~0.05. (b) The observed 1/1 double tearing modes with different m numbers, when the current blip was scanned from the core of the plasma toward the q=1 surface, are consistent with the calculated growth rates of the same modes for the current blip with equilibrium q-profile with q_0=1.04.

5.2. PLASMA FLOW AND TURBULENCE IN THE PRESENCE OF MAGNETIC ISLANDS

The dynamics of the plasma flow and electron temperature (T_e) turbulence surrounding the macroscopic m/n=2/1 magnetic island were measured with the 2D ECEI system in an L-mode discharge #13371 [32]. A rigorous analysis showed that the distribution of T_e fluctuations is highly inhomogeneous around the island and no fluctuations were measured inside the island as shown in Fig. 13. The fluctuations are mostly concentrated in a region near the X-point of the magnetic island as shown in this figure. On the other hand, the poloidal flow shears are strongest near the O-point of the island, which is an opposite trend to that of the fluctuations as shown in this figure. Global gyrokinetic simulations were carried out to investigate the underlying physics of the

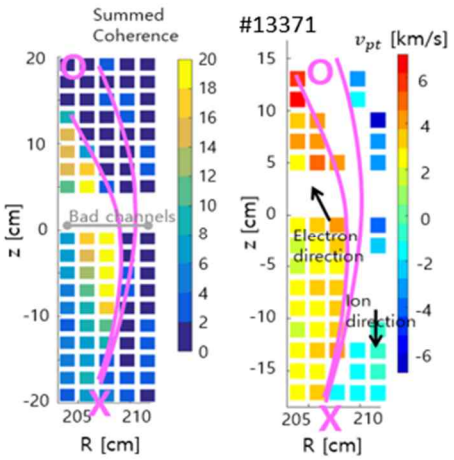

Fig. 13. T_e fluctuation distribution (left) and apparent poloidal flow (right) around a (2,1) magnetic island. The magenta curves indicate to the separatrix of the magnetic island, and O and X indicate the O- and X-point direction of the island, respectively.

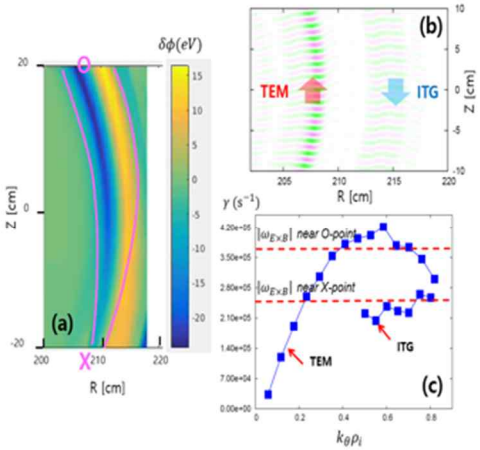

Fig. 14. (a) The perturbed equilibrium potential from XGC1, (b) the contours of micro-instabilities around the magnetic island in the outer mid-plane, and (c) the comparison of the ExB shearing rates at the O- and X-point of the magnetic island and the growth rates of the micro-instabilities.

measured flow and fluctuation patterns [33]. The global equilibrium ExB flow perturbed by the m/n=2/1 island was calculated using XGC1 code as shown in Fig. 14 (a). It was found that the flowing shear is maximum and minimum near the O- and X-point of the island, respectively. From global micro-instability analyses using gKPSP code, it was found that collisionless trapped electron mode (CTEM) and ion temperature gradient (ITG) mode can be excited around the island as shown in Fig. 14 (b). However, due to the strong shear of the ExB flow, a significant portion of CTEM is suppressed in the region near the O-point as shown in Fig. 14 (c). On the other hand, the flow shear around the X-point is not strong enough to stabilize ambient instabilities, which is consistent with the experimental measurements shown in Fig. 13.

5.3. DYNAMICS AND CONTROL OF ELMS AND ELM-CRASH USING MAGNETIC PERTURBATIONS

Since the first successful suppression experiment of the ELM-crash using RMP coils [34], exploration of the ELM-crash suppression mechanisms has been the prime research subject and various experiments using a combination of the phase and amplitude of RMP and NRMP have been conducted to expand the operational window of the ELM-crash suppression without much loss of confinement. The role of critical physical parameters, such as q_{95}, δ, and ν∗ were extensively investigated. However, all these critical parameters are interrelated through the plasma response and it is somewhat difficult to isolate the responsible parameters for the mechanism of suppression. As a results, empirical exercise on the ELM-crash control experiment revealed more questions than answers. In parallel, modeling of penetrating non-axisymmetric field of the applied RMPs including in the presence of the plasma has made a significant progress.

In 2016, KSTAR showed that MHD modeling for multi-resonant coupling can be used to predict the n=1 RMP operational windows for ELM-crash suppression in a complicated KSTAR coil phase space [7]. This extrapolation has been extended to the RMPs with n=2 which has been equally effective in suppression of the ELM-crash in a limited condition (e.g. $3.3<q_{95}<4.1$) but less reliable compared to the n=1 RMPs. The modeled phase space diagrams in Fig. 15 provide good explanations. The diagrams illustrates the n=2 RMP window for ELM control in blue, in which the edge RMP is strong (otherwise in green) while the core RMP is weak (otherwise in red) with

respect to each resonant bifurcation threshold. It is represented on a 2-D subset of coil phase space where all 3 internal rows of coils have the same n=2 currents in amplitude, and the same phase shift for upper and lower part of coils. The (orange) horizontal bar indicates the space where the present KSTAR coils can access. It is clear that the phase shift that the KSTAR coils can presently compose (either 0° or 90°) is not optimal, and that the edge coupling becomes too weak for q_{95}>4.2 within the 5kA current capability of the IVCC while the core coupling becomes too strong for q_{95}<3.0. It is possible to extend the q_{95} window by optimizing target shapes, rotation, or choosing a different subset of coils, but in general new capability to rotate the n=2 toroidal phase would be beneficial for KSTAR. The KSTAR research team will continue to explore such new coil concepts, including an innovative ex-vessel RMP solution to maintain the RMP feasibility in a reactor environment. The proposed method will be used to efficiently predict the various RMP options and coupling in response, once it is combined with reliable RMP bifurcation models and/or empirical projections.

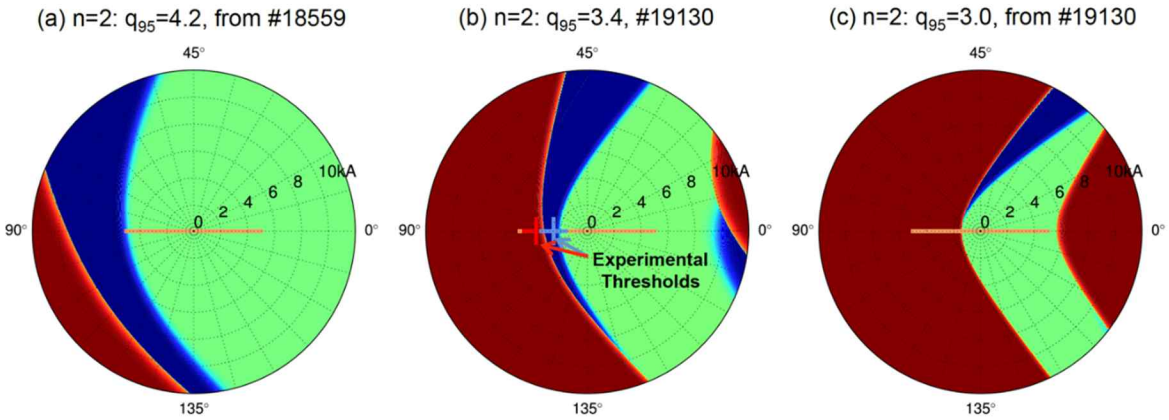

Fig 15. The phase space diagrams showing the n=2 RMP (blue) windows for ELM-crash suppression for different q_{95} plasmas, on a 2D subset of KSTAR coil phase space where the n=2 currents are same for all 3 rows of coils and the phase shift for upper and lower part between neighboring rows is also same. The red zone is where the core locking is predicted, and the green zone is where the resonant response is predicted to be weak. The window is presently accessible (orange horizontal bar, 0~5kA with 0° or 90° phase shift) only for (b) q_{95}=3.4, where the empirical thresholds for ELM-crash suppression (blue +) and for locking threshold (red +) are indeed found consistent with the prediction.

The first direct measurement of the radially localized electron temperature (T_e) turbulence was made in addition to the coherent ELM fluctuation during the ELM-crash suppression experiment in the presence of RMPs as illustrated in Fig. 16(a) [13]. In this work, a reduction of the ELM amplitude (blue symbol) and increase of the low frequency turbulence (red symbol) presumably induced by the applied RMP current (gold) through non-linear interaction are demonstrated as the RMP current is ramped up as shown in this figure. The low frequency turbulence represents stochastic islands generated by the penetrated non-axisymmetric fields takes the energy of the coherent ELMs through non-linear interaction. The increase of the turbulence may contribute to the local viscosity change and hence the poloidal rotation of the plasma flow. In recent experiments [14], the study of turbulence induced by RMP has further advanced and demonstrated that the

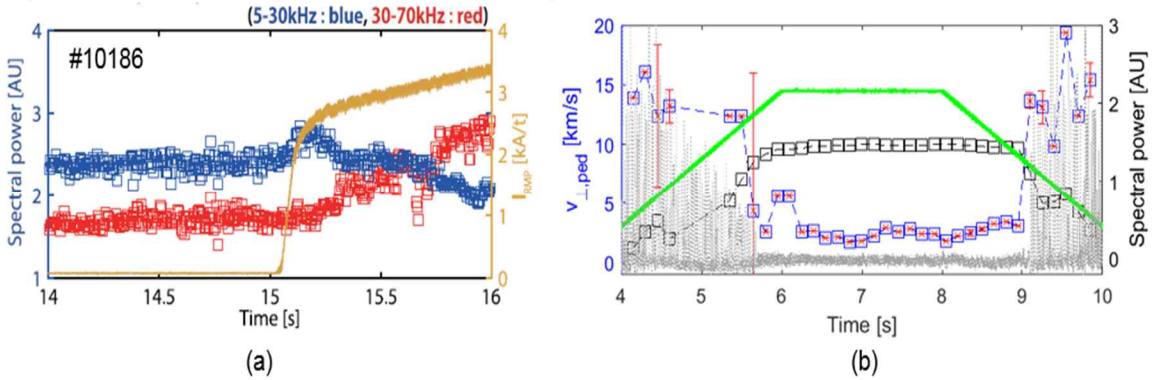

Fig. 16. (a) Anti-correlation between amplitude of the ELMs (blue) and turbulence amplitude (red) is demonstrated during RMP experiment. (b) Turbulence amplitude (black box) and $V_\perp$ change (blue box) are shown with the ELM phase transition and with the n=1 RMP field strength (green line).

increase of the turbulence amplitude (black box) is well correlated with the RMP current ramp up (green line) while the amplitude of the ELM-crash is gradually reduced and finally made transition to the ELM-cash suppression as the amplitude of the turbulence is about to saturate as illustrated in Fig. 14(b). Also the measured perpendicular turbulence flow ($V_\perp$) (blue box) is suddenly stalled at the transition time. In the ramp down period, there is a clear time delay between the RMP current and decay of the amplitude of the turbulence. A sudden increase of $V_\perp$ is notable at the end of the suppression period. The observed delay may come from a long decay time of the perturbed magnetic fields (order of ~1s for λ~1.5 cm from reference 13). Also the on-set of the ELM-crash is clear as the turbulence amplitude is reduced while $V_\perp$ is accelerated. If the amplitude of the turbulence is an indication of stochastic islands due to the penetrated 3D fields, the growth of the stochastic islands may slow the turbulence flow through the increased viscosity and nonlinear interaction between the ELM and induced turbulence inhibits the ELM-crash when the growth of the ELM is below a critical value. Further study of the relationship between the amplitude of turbulence and $V_\perp$ is in progress to understand the underlying physics of correlation and anti-correlation of these critical parameters (turbulence amplitude, $V_\perp$, and ELM-crash mitigation and/or suppression) [14].

5.4. TRANSPORT PHYSICS BASED ON TURBULENCE

Using the 2-D pixels of microwave imaging systems (ECEI and MIR), measured electron turbulence (both T_e and n_e) has been extensively analyzed to support the transport physics as well as the role of turbulence in MHD as discussed in the previous section. Here, the advantage of the 2D nature of the measurement has been fully

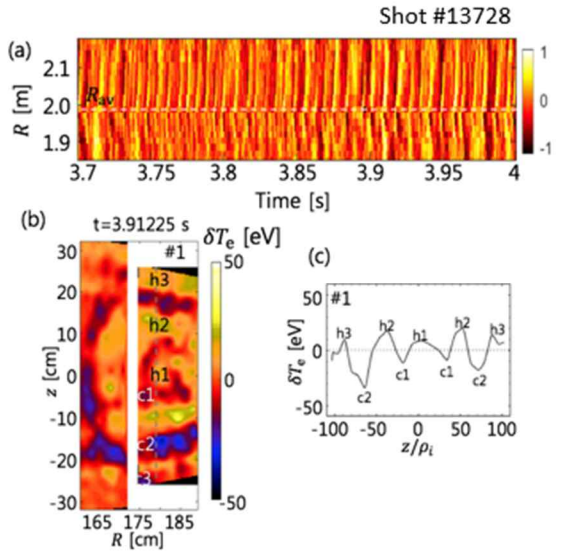

Fig. 17. (a) Voids and bumps are observed in the spatio-temporal pattern of the T_e fluctuation. (b) The electron temperature profile corrugations are clearly observed via the $\delta T_e = T_e - \langle T_e \rangle$ image in between the long range avalanche-like events. (c) Vertical cuts of δT_e along the plasma center.

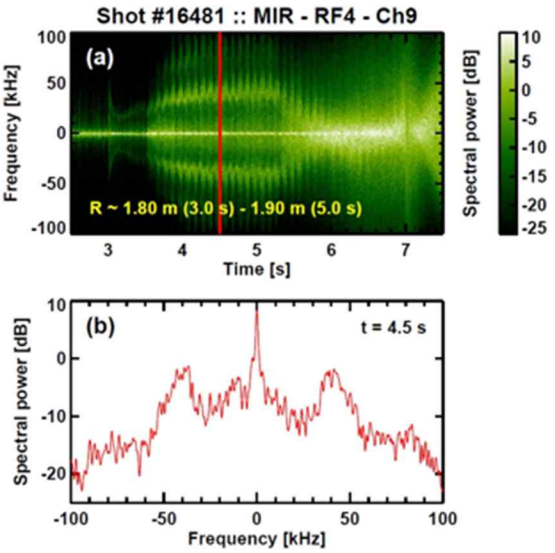

Fig. 18. (a) A spectrogram of density fluctuations of the MIR channels (RF4-ch9) in the core region is shown for the ECH assisted discharge #16481the core region (b) A typical spectrum of QCM at 4.5 s is illustrated.

exploited to address the global and local physics associated with the turbulence in the plasmas. As the first example, "avalanche" [32] event is a fast non-diffusive transport event due to successive increase of fluctuation intensity as the heat front propagates. In KSTAR, a long-range avalanche-like electron heat transport event is observed in the MHD-quiescent L-mode plasma without any external perturbations and an example is shown in Fig. 17(a) [15]. Voids and bumps, propagating inwards and outwards from the position of $R_{av} \sim 1.96$m, are observed and satisfied the criterion of joint reflection symmetry (JRS) [35]. The propagation speed is about 90 m/s, which is much faster than typical velocities involved in diffusive processes. Interestingly, this long range avalanche-like event occurs only when the T_e profile corrugations vanish. This is an indication of destruction of the shear flow layers. Fig. 17(b) shows the T_e profile corrugations observed in between the events. The measured spacing of the profile corrugations is roughly $45\rho_i$ which agrees well with the most probable spacing observed in previous

simulations [36]. Two ion-gyroscale ($0.1 < k_{\perp}\rho_i < 1$) micro-instabilities are often dominant in core region of the tokamak plasmas. They are ITG modes and trapped electron modes (TEMs). The identification of micro-instability type is important since it was reported that two micro-instabilities provide different (or contrary) effects on the plasma parameters, intrinsic rotation, and nonlocal transport. However, the identification is not always possible due to their similar scales and spectral distribution. Recently, it was reported that the density fluctuation spectrum measured in ohmic plasmas demonstrated a distinctive spectral structure referred to as the quasi-coherent mode (QCM) and the mode has been active in TEM dominant plasmas [37]. With the microwave imaging reflectometer (MIR) [6], properties of QCM were studied in KSTAR ohmic (and ECH assisted) plasmas [16]. Fig. 18(a) illustrates that a QCM at f_{peak} = 40 kHz appears at about ~3.5s in the core region of an ECH discharge #16481 when ECH is injected from 3s in the low density plasma and the QCM is suppressed by increased density (or collisionality). A typical spectrum of the QCM is also shown in Fig. 18(b).

6. FUTURE RESEARCH PLAN TOWARD ITER AND K-DEMO

Valuable experience in operation of the superconducting tokamak and accumulation of new knowledge from physics research will allow access to higher beta steady state operation with additional heating power in NBI (total up to 12 MW) and ECH (total up to 6 MW). The performance goal of high performance plasma at β_N>3 with T_i~10 keV and bootstrap fraction (f_{bs})>0.5 may be feasible and predicted by TRANSP runs [38]. The improved performance of the conventional advanced mode of operation such as (high β_P, hybrid, ITB, low q95, etc.) will be integrated with smart control capability of the harmful MHDs to minimize disruption. At the same time, new alternative mode of operation, core confinement with broader ITB foot at low edge q_{95}~2.2 will be pursued to minimize the harmful MHDs while the confinement is comparable to that of the conventional H-mode. In order to accommodate the anticipating increased plasma performance, upgrade plan for new divertor

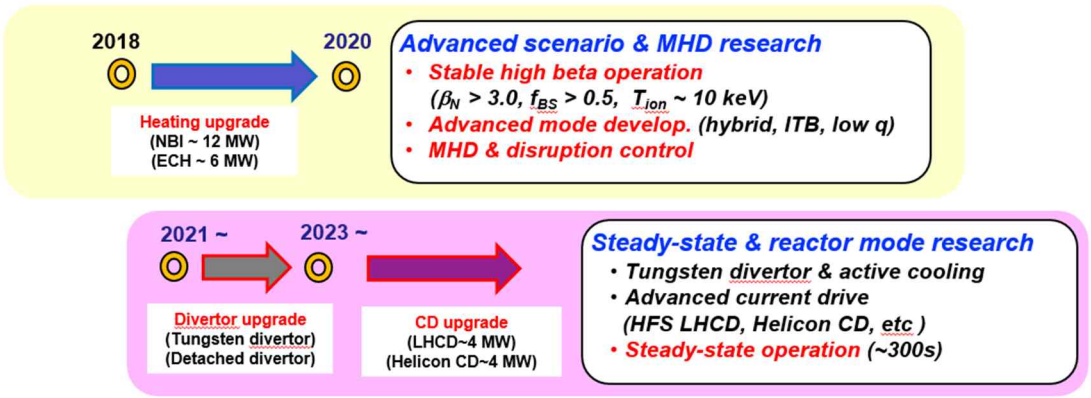

Fig. 19. Flow chart of KSTAR operation plan and divertor upgrade plan. Until 2020, advanced scenario for stable high beta plasma operation will be continued with the new 2nd NBI system. Upgrade plan for new divertor and internal hardware is planned in ~2021 and stable steady state higher beta operation will be continued with an efficient current drive system

system and internal structures vulnerable to the higher heat flux is in preparation now. The internal hardware upgrade will be followed by experiences in stable higher beta long pulse operation with the 2nd NBI system which will be completed in 2019 and execution of the upgrade plan would be around ~2021 as shown in Fig. 19. Here, emphasis will be placed on a new actively cooled tungsten divertor with new first wall materials. In order to assess the feasibility of metal wall materials in the KSTAR upgrade plan, experiments using specially designed castellated tungsten block tiles of various shapes have been performed in support of multi-machine (ITPA) efforts to understand power loading on leading edges in the ITER divertor [39]. Besides, impurity transport physics experiments have been conducted with the injection of trace Ar and Kr gases and tungsten dust, addressing the dependence of ECH and magnetic perturbation on the impurity accumulation at the plasma core.

For preparation of the current drive system on KSTAR, Helicon wave current drive will be tried. In previous campaigns, the low power system (~100 kW) was tested and results were encouraging. Currently a high power

system utilizing klystron tube at ~500MHz with ~4MW high power klystron is under development. As a back-up plan, a conventional LHCD system will be implemented for additional current drive for steady state application. The improved capacity of an ancillary system such as a tungsten divertor system and accumulated knowledge of plasma operation warrants to develop and demonstrate steady state operation up to 300s which has been the goal of KSTAR. A potential mode of operation including new low q_{95} mode, which can eliminate NTM and ELMs while the confinement is comparable to the H-mode, for K-DEMO will be fully exploited so that the design effort of K-DEMO can be benefited.

ACKNOWLEDGEMENTS

*This work is supported by the KSTAR research project funded by Korea Ministry of Science, ICT and Future Planning and NRF under contract number NRF-2014M1A7A1A03029865.

REFERENCES

[1] G.S. LEE, et al., Nucl. Fusion, **41**, 1515 (2001)
[2] J.G. Kwak, et al., Nucl. Fusion, **53**, 104005 (2013)
[3] Y. In, et al., Nucl. Fusion, **55**, 043004 (2015)
[4] H.L. Yang, et al, Fusion Engineering and Design, **86,** Issues 6–8, 588-592 (2011)
[5] G.S. Yun, et al., Rev. Sci. Instrum., **81** 10D930 (2010)
[6] W. Lee, et al., Nucl. Fusion, **54**, 023012 (2014)
[7] J.K. Park, https://doi.org/10.1038/s41567-018-0268-8, Nature Physics (2018)
[8] W.H. Ko, et al., APS bulletin (2017)
[9] Y. Nam, et al., Nucl. Fusion, **58**, 066009 (2018)
[10] G.H. Choi, et al., to be published in Nucl. Fusion (2018)
[11] M.J. Choi, et al., Nucl. Fusion, **57**, 126058 (2017)
[12] J.M. Kwon, et al., ibid (2018)
[13] J. Lee, et al., Phy. Rev. Lett., **117,** (7) 075001 (2016)
[14] J. Lee, et al., ibid (2018)
[15] M. Choi, et al., arXiv:1806.04947 v2 (2018),
[16] J. A. Lee, *et al.*, Phys. Plasmas **25**, 022513 (2018).
[17] R.J. La Haye, et al., Phys. Fluids, **B4** 1813 (2003)
[18] J.E. Menard et al., Nucl. Fusion, **50**, 045008 (2018)
[19] M. Yoo, et al., Nature Commun. 9 3523 (2018)
[20] J. Lee et al., Nucl. Fusion, 57 126033 (2017)
[21] J. Chung, et al., Nucl. Fusion, 58, 016019 (2018)
[22] S. Sabbagh, et al., ibid (2018)
[23] Y. In, et al., ibid (2018)
[24] K.C. Shaing, et al., Nucl. Fusion, **55,** 125001 (2015)
[25] S.A. Sabbagh, et al., 44th EPS conference paper P1.164 (2017)
[26] A.R. Polevoi, et al., Nucl. Fusion, **45,** 1454 (2005)
[27] H. Soltwisch, et al., Rev. Sci. Instrum., **59**, 1599 (1988)
[28] D. Wroblewski, et al., Phy. Rev. Lett., **71**, 859 (1993)
[29] B. Kadomtsev, et al., Sov. J. Plasma Phys., **1**, 389 (1975)
[30] J. Ko, et al., Rev. Sci. Instrum., **87** 11E541 (2016)
[31] Z. Chang, et al., Phy. Rev. Lett., **77**, 3553, (1996)
[32] M.J. Choi, et al., ibid (2018)
[33] J.M. Kwon, et al., Phys. Plasmas, **25**, 052506 (2018)
[34] T.E. Evans, et al., Phys. Rev. Lett., **23**, 235003 (2004)
[35] G. Dif-Pradalier, et al., Nucl. Fusion, **57**, 066026 (2017)
[36] P.H. Diamond, et al., Phys. Plasmas, **2**, 3640 (1995)
[37] H. Arnichand, et al., Nucl. Fusion, **55**, 093021 (2015).
[38] Y.S. Park, et al., ibid (2018)
[39] S.H. Hong, et al., ibid (2018)